



The influence of convection on OH UV line formation in the atmosphere of the metal-poor red giant HD 122563

D. Prakapavičius¹, A. Kučinskas^{1,2}, V. Dobrovolskas¹, J. Klevas¹, M. Steffen^{3,4},
P. Bonifacio⁴, H.-G. Ludwig^{5,4}, and M. Spite⁴

- ¹ Institute of Theoretical Physics and Astronomy, Vilnius University, Saulėtekio al. 5, Vilnius LT-10221, Lithuania, e-mail: dainius.prapakavicius@tfai.vu.lt
² Astronomical Observatory, Vilnius University, M. K. Čiurlionio 29, Vilnius LT-03100, Lithuania
³ Leibniz-Institut für Astrophysik Potsdam, An der Sternwarte 16, D-14482 Potsdam, Germany
⁴ GEPI, Observatoire de Paris, PSL Research University, CNRS, Place Jules Janssen, 92190 Meudon, France
⁵ Landessternwarte – Zentrum für Astronomie der Universität Heidelberg, Königstuhl 12, D-69117 Heidelberg, Germany

Abstract. We utilized high-resolution spectra of the metal-poor red giant star HD 122563 and classical 1D hydrostatic ATLAS9 model atmosphere to derive the 1D LTE oxygen abundance from OH UV lines. The obtained average 1D LTE oxygen abundance is $\langle A(\text{O})_{1\text{D LTE}} \rangle = 6.41 \pm 0.16$. We also used 3D hydrodynamical CO5BOLD and 1D hydrostatic LHD model atmospheres to correct the 1D LTE abundances for convection-related effects and to determine average 3D LTE abundance, $\langle A(\text{O})_{3\text{D LTE}} \rangle = 6.23 \pm 0.13$. We found that while the oxygen abundances determined using 1D hydrostatic model atmospheres showed trends both with the line strength and excitation potential, these trends essentially disappeared in the 3D LTE case. The average 3D LTE oxygen abundance obtained from the OH UV lines agrees reasonably well with the oxygen abundances obtained in the earlier analyses from the OH IR lines and the 630.0 nm [O I] line, while the remaining small discrepancies may possibly be attributed to NLTE effects.

Key words. Stars: atmospheres – Stars: late-type – Stars: individual (HD 122563) – Convection – Hydrodynamics

1. Introduction

Aoki (2015) has reported that 1D LTE oxygen abundances in the metal-poor subgiant BD+44°493 determined from molecular OH lines located in the UV part of the spectrum (310–330 nm) were dependent on vari-

ous spectral line parameters, such as excitation potential, χ , and equivalent width, W . These dependencies may indicate potential problems with the 1D hydrostatic model atmospheres that were used in abundance determinations, or inadequacies of 1D LTE techniques, or both, thus the author suggested that the applica-

tion of 3D hydrodynamical model atmospheres might help to alleviate these problems. It has been also debated that oxygen abundances determined with the 1D model atmospheres using different abundance indicators (e.g., forbidden oxygen line at 630.0 nm, OH lines in the UV and IR) may differ significantly (e.g., Barbuy et al. 2003; Asplund et al. 2004). In this contribution we therefore use 1D hydrostatic and 3D hydrodynamical model atmospheres to analyse OH UV spectral lines in a high-resolution archival VLT UVES spectrum of the bright ($V = 6.2$) metal-poor giant HD 122563 (program ID 266.D-5655) and to investigate whether application of the 3D hydrodynamical model atmospheres may help to resolve these standing issues.

In Sect. 2 of this contribution we briefly describe the methods of 1D LTE and 3D LTE abundance analysis. In Sect. 3 we present oxygen abundances determined using different model atmospheres and provide a grid of 3D–1D abundance corrections. Our main findings and conclusions are summarized in Sect. 4. We also refer to Prakapavičius et al. (2017) for a more detailed discussion.

2. Methodology

We used a high-resolution ($R = 60\,000$) spectrum of HD 122563 which was observed with the UVES spectrograph. A reduced spectrum was taken from the UVES-POP archive (program ID 266.D-5655; Bagnulo et al. 2003) and was subsequently normalized. 1D LTE oxygen abundances, $A(\text{O})_{\text{1D LTE}}^i$ for each considered OH UV spectral line i , were determined by adjusting synthetic line profiles to match those in the observed spectrum of HD 122563. For the computation of synthetic line profiles we used classical 1D ATLAS9 model atmosphere (Sbordone et al. 2004; Sbordone 2005) characterized by the following atmospheric parameters: $T_{\text{eff}} = 4600$ K and $\log g = 1.60$ (both taken from Creevey et al. 2012), and $[\text{Fe}/\text{H}] = -2.60$ (Mashonkina et al. 2011). We then used 1D LTE SYNTHE spectral synthesis package (Sbordone et al. 2004; Sbordone 2005) and computed a grid of synthetic line profiles that in case of each spectral line were

defined by two grid parameters: oxygen abundance, $A(\text{O})_{\text{1D LTE}}^i$, and broadening velocity, v_{brd}^1 . In this step we used the microturbulence velocity of $\xi_{\text{mic}} = 2.0$ km/s, as determined by Spite et al. (2005). Subsequently, we have applied χ^2 minimization technique to find the synthetic line profiles that provided the best fit to those observed in the spectrum of HD 122563. The result of this procedure were oxygen abundances, $A(\text{O})_{\text{1D LTE}}^i$, obtained from each individual OH UV line.

The 3D LTE abundances were obtained by adding 3D–1D oxygen abundance corrections, $\Delta_{\text{3D-1D}}^i$, to $A(\text{O})_{\text{1D LTE}}^i$ abundances determined using individual OH UV lines. Curves of growth (COGs) used in this procedure were computed using 3D hydrodynamical CO5BOLD (Freytag et al. 2012) and 1D hydrostatic LHD (Caffau et al. 2008) model atmospheres, in both cases with identical atmospheric parameters ($T_{\text{eff}} = 4600$ K, $\log g = 1.60$, $[\text{Fe}/\text{H}] = -2.50$), chemical composition, and equation of state, to ensure strictly differential analysis. All COGs were computed using Linfor3D spectral synthesis package³. Importantly, in this step we used ξ_{mic} that was determined from the 3D hydrodynamic model atmosphere using Method 1 of Steffen et al. (2013), $\xi_{\text{mic}} = 1.30$ km/s. Although this value is somewhat lower than that determined in the classical 1D LTE abundance analysis and used by us to determine 1D LTE oxygen abundance from OH UV lines ($\xi_{\text{mic}} = 2.0$ km/s, Spite et al. 2005), we believe that our approach allows us to compensate for the shortcomings in the current 3D hydrodynamical model atmospheres (see Steffen et al. 2013; Prakapavičius et al. 2017, Appendix C).

¹ We used the broadening velocity, v_{brd} , to account for the cumulative effect of macroturbulence, stellar rotation, and instrumental broadening.

² The 3D–1D abundance correction, $\Delta_{\text{3D-1D}}^i$, is a difference in the oxygen abundance determined using 3D hydrodynamical and 1D hydrostatic model atmospheres from the same spectral line of a given W_i .

³ <http://www.aip.de/Members/msteffen/linfor3d>

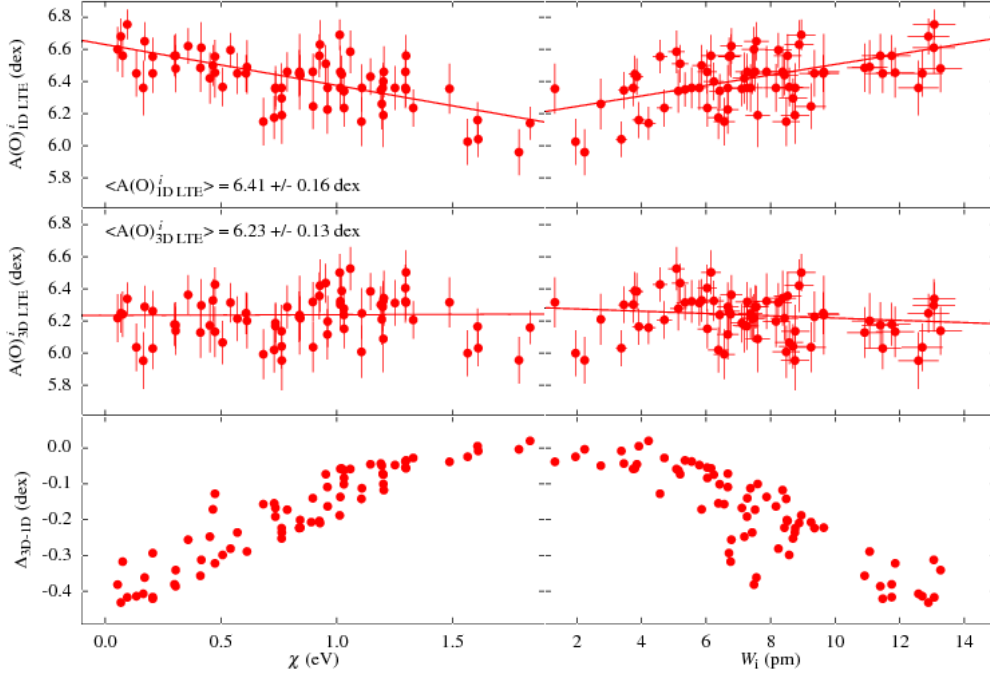


Fig. 1. Oxygen abundances determined from individual OH UV lines using a 1D hydrostatic ATLAS9 model atmospheres (top row), those corrected for 3D hydrodynamical effects using C05B0LD and LHD model atmospheres (middle row), and 3D–1D oxygen abundance corrections for each spectral line (bottom). The quantities are plotted against the line excitation potential, χ (left column), and line equivalent width, W_i (right column). The error bars denote quadratically summed errors that come from a variety of relevant sources (line profile fitting, continuum placement, uncertainties in the atmospheric parameters, and W measurement).

3. Results

We have used 71 OH spectral lines located in the UV part of the spectrum (310–330 nm) to derive the average 1D LTE and 3D LTE oxygen abundances, $\langle A(O)_{1D LTE}^i \rangle = 6.41 \pm 0.16$ and $\langle A(O)_{3D LTE}^i \rangle = 6.23 \pm 0.13$ (the average abundances were obtained as error-weighted means; the errors are standard deviations resulting from the spread in individual abundances determined from different spectral lines). In the top row of Fig. 1 we show $A(O)_{1D LTE}^i$ plotted versus χ and W_i . One may notice that 1D LTE abundances clearly depend on both χ and W_i though these trends essentially vanish when the 3D LTE abundances are used instead (Fig. 1, middle row).

Table 1. Oxygen abundances determined from OH UV, OH IR, and atomic [O I] lines using 1D hydrostatic and 3D hydrodynamical model atmospheres. Oxygen abundances obtained from OH IR lines were taken from Dobrovolskas et al. (2015) and those determined using the forbidden [O I] line from Spite et al. (2005).

	A(O)	
	1D LTE	3D LTE
OH UV	6.41 ± 0.16	6.23 ± 0.13
OH IR	6.63 ± 0.10	6.39 ± 0.11
[O I]	6.54 ± 0.15	6.53 ± 0.15

Bottom row of Fig. 1 shows that the largest (most negative) 3D–1D abundance corrections

Table 2. A grid of derived 3D–1D abundance corrections, Δ_{3D-1D}^i , for fictitious OH UV lines characterized with different wavelength, λ , excitation potential, χ , and line equivalent width, W . The abundance corrections were derived using model atmospheres defined by $T_{\text{eff}} = 4600$ K, $\log g = 1.60$, $[\text{Fe}/\text{H}] = -2.50$.

χ/eV		0.0	0.4	0.8	1.2	1.6	2.0
$\log(W/\text{pm})$	W, pm	$\lambda = 306 \text{ nm}$					
0.0	1.00	-0.210	-0.151	-0.101	-0.057	-0.010	0.012
0.2	1.58	-0.199	-0.142	-0.092	-0.050	-0.014	0.018
0.4	2.51	-0.185	-0.130	-0.083	-0.041	-0.004	0.029
0.6	3.98	-0.193	-0.133	-0.081	-0.035	0.005	0.042
0.8	6.31	-0.334	-0.240	-0.158	-0.087	-0.024	0.032
1.0	10.0	-0.539	-0.388	-0.259	-0.151	-0.060	0.015
1.2	15.8	-0.368	-0.259	-0.168	-0.092	-0.028	0.026
		$\lambda = 318 \text{ nm}$					
0.0	1.00	-0.213	-0.155	-0.105	-0.062	-0.026	0.006
0.2	1.58	-0.201	-0.145	-0.097	-0.056	-0.020	0.011
0.4	2.51	-0.187	-0.133	-0.085	-0.045	-0.010	0.021
0.6	3.98	-0.182	-0.126	-0.077	-0.035	0.002	0.035
0.8	6.31	-0.280	-0.198	-0.128	-0.067	-0.013	0.036
1.0	10.0	-0.499	-0.358	-0.239	-0.138	-0.054	0.017
1.2	15.8	-0.370	-0.260	-0.170	-0.094	-0.031	0.022
		$\lambda = 330 \text{ nm}$					
0.0	1.00	-0.218	-0.160	-0.111	-0.069	-0.033	-0.001
0.2	1.58	-0.207	-0.151	-0.104	-0.062	-0.027	0.004
0.4	2.51	-0.192	-0.138	-0.093	-0.053	-0.018	0.013
0.6	3.98	-0.182	-0.129	-0.083	-0.042	-0.006	0.027
0.8	6.31	-0.252	-0.179	-0.117	-0.062	-0.013	0.030
1.0	10.0	-0.468	-0.337	-0.227	-0.133	-0.055	0.013
1.2	15.8	-0.379	-0.268	-0.176	-0.101	-0.038	0.014

were derived for the spectral lines characterized by the lowest χ and highest W_i . As it was pointed out earlier in, e.g., Dobrovolskas et al. (2013), formation of molecular lines in the atmospheres of metal-poor stars takes place in their outer layers that are characterized by strong horizontal temperature inhomogeneities. The effect of these inhomogeneities is thus largest in case of strong low-excitation lines since these lines form in the outermost layers, which leads to large and negative Δ_{3D-1D}^i . The obtained results therefore indicate that the adequate modelling of the horizontal inhomogeneities (which is only possible with the 3D hydrodynamical model atmospheres) is crucial for the reliable abundance analysis based on molecular lines.

In Table 1 we provide 1D/3D LTE oxygen abundances determined in HD 122563 using

three different indicators: OH UV lines (this work), OH IR lines (taken from Dobrovolskas et al. 2015), and the forbidden [O I] line at 630.0 nm (taken from Spite et al. 2005). A comparison of these values suggests that the mean abundances determined using OH UV and IR lines agree slightly better in 3D LTE as the abundance difference between the two diminishes from 0.22 dex in 1D LTE to 0.16 dex in 3D LTE. Unfortunately, the same can not be said about the abundances obtained from molecular lines and atomic [O I] 630.0 nm line: in this case, the agreement is slightly worse in 3D LTE⁴. This result may point out to the pos-

⁴ Note that the 3D–1D abundance correction for atomic [O I] 630.0 nm line is small (≤ 0.01 dex) and it is thought that this line is not sensitive to non-LTE effects (see, e.g., Asplund et al. 2004).

sible influence of non-LTE effects on the formation of OH UV lines which, via non-local radiation field, may increase photodissociation rates of OH molecules and subsequently weaken their spectral lines. Accounting for these effects may therefore yield higher oxygen abundances obtained using OH UV lines and may thus bring them into better agreement with the oxygen abundance obtained using the forbidden [O I] line at 630.0 nm.

To facilitate the future 3D LTE oxygen abundance analyses based on OH UV lines in HD 122563, we computed a grid of 3D–1D abundance corrections for a set of fictitious OH UV lines characterized by different line parameters: $0.0 < \chi/\text{eV} < 2.0$ (in steps of 0.4), $0.1 < \log(W/\text{pm}) < 0.22$ (in steps of 0.02), and $\lambda = 306, 318, \text{ and } 330 \text{ nm}$. The 3D–1D abundance corrections are provided in Table 2 and they can be interpolated to any set of line parameters that fall within the parameter range above.

4. Conclusions

We determined 1D/3D LTE oxygen abundances in the metal-poor red giant HD 122563 using 71 OH lines located in the UV part of the spectrum (310–330 nm). For this, we used classical 1D hydrostatic (ATLAS9 and LHD) and 3D hydrodynamical C05B0LD model atmospheres. The obtained average abundances are $\langle A(\text{O})_{1\text{D LTE}}^i \rangle = 6.41 \pm 0.16$ and $\langle A(\text{O})_{3\text{D LTE}}^i \rangle = 6.23 \pm 0.13$. Oxygen abundances derived with the ATLAS9 model atmospheres showed significant trends with the line excitation potential and equivalent width but these trends essentially disappeared in the 3D LTE case. In addition, 3D LTE modelling helped to bring oxygen abundances determined from OH UV and IR spectral lines into somewhat better agreement. Unfortunately, the difference between the 3D LTE oxygen abundance obtained from OH UV lines ($\langle A(\text{O})_{1\text{D LTE}}^i \rangle = 6.41 \pm 0.16$) and that determined from the forbidden [O I] 630.0 nm line ($A(\text{O}) = 6.53 \pm 0.15$) became slightly worse. The latter result may signal about the influence of non-LTE effects on the OH UV spectral line formation. Despite this

minor disagreement, our results indicate that 3D hydrodynamical models of metal-poor red giant stars are crucial for reliable determination of oxygen abundances using OH UV lines.

Acknowledgements. This work was supported by grant from the Research Council of Lithuania (MIP-089/2015). DP acknowledges financial support from Vilnius University that allowed to visit the 3rd C05B0LD Workshop. JK thanks the organizers of the 3rd C05B0LD Workshop for the financial assistance that helped to attend the event. HGL acknowledges financial support by Sonderforschungsbereich SFB 881 "The Milky Way System" (subproject A4) of the German Research Foundation (DFG). A part of computations were performed at the High Performance Computing Center, HPC Sauletekis, of the Faculty of Physics, Vilnius University.

References

- Aoki, W. 2015, *ApJ*, 811, 64
 Asplund, M., Grevesse, N., Sauval, A. J., et al. 2004, *A&A*, 417, 751
 Bagnulo, S., Jehin, E., Ledoux, C., et al. 2003, *Messenger*, 114, 10
 Barbuy, B., Meléndez, J., Spite, M., et al. 2003, *ApJ*, 588, 1072
 Caffau, E., Ludwig, H.-G., Steffen, M., et al. 2008, *A&A*, 488, 1031
 Creevey, O. L., Thévenin, F., Boyajian, et al. 2012, *A&A*, 545, 17
 Dobrovolskas, V., Kučinskas, A., Steffen, M., et al. 2013, *A&A*, 559, A102
 Dobrovolskas, V., Kučinskas, A., Bonifacio, P., et al. 2015, *A&A*, 576, A128
 Freytag, B., Steffen, M., Ludwig, H.-G., et al. 2012, *J. Comp. Phys.*, 231, 919
 Mashonkina, L., Gehren, T., Shi, et al. 2011, *A&A*, 528, A87
 Prakapavičius, D., Kučinskas, A., Dobrovolskas, V., et al. 2017, *A&A*, 599, A128
 Sbordone, L., Bonifacio, P., Castelli, F., et al. 2004, *MSAIS*, 5, 93
 Sbordone, L. 2005, *MSAIS*, 8, 61
 Steffen, M., Caffau, E., & Ludwig, H.-G. 2013, *MSAIS*, 24, 37
 Spite, M., Cayrel, R., Plez, B., et al. 2005, *A&A*, 430, 655